JACS
JOURNAL OF THE AMERICAN CHEMICAL SOCIETY
pubs.acs.org/JACS
Article

Synthesis of Nitro Compounds from Nitrogen Dioxide Captured in a Metal-Organic Framework

Jiangnan Li, Zi Wang, Yinlin Chen, Yongqiang Cheng, Luke L. Daemen, Floriana Tuna, Eric J. L. McInnes, Sarah J. Day, Anibal J. Ramirez-Cuesta, Martin Schröder,* and Sihai Yang*

Cite This: J. Am. Chem. Soc. 2022, 144, 18967−18975

ABSTRACT: Increasing levels of air pollution are driving the need for the development of new processes that take "waste-to-chemicals". Herein, we report the capture and conversion under ambient conditions of a major air pollutant, NO_2, using a robust metal-organic framework (MOF) material, Zr-bptc (H_4bptc = 3,3′,5,5′-biphenyltetracarboxylic acid), comprising $\{Zr_6(\mu_3\text{-}O)_4(\mu_3\text{-}OH)_4(COO)_{12}\}$ clusters linked by 4-connected $bptc^{4-}$ ligands in an **ftw** topology. At 298 K, Zr-bptc shows exceptional stability and adsorption of NO_2 at both low (4.9 mmol g^{-1} at 10 mbar) and high pressures (13.8 mmol g^{-1} at 1.0 bar), as measured by isotherm experiments. Dynamic breakthrough experiments have confirmed the selective retention of NO_2 by Zr-bptc at low concentrations under both dry and wet conditions. The immobilized NO_2 can be readily transformed into valuable nitro compounds relevant to construction, agrochemical, and pharmaceutical industries. *In situ* crystallographic and spectroscopic studies reveal strong binding interactions of NO_2 to the $\{Zr_6(\mu_3\text{-}O)_4(\mu_3\text{-}OH)_4(COO)_{12}\}$ cluster node. This study paves a circular pathway to enable the integration of nitrogen-based air pollutants into the production of fine chemicals.

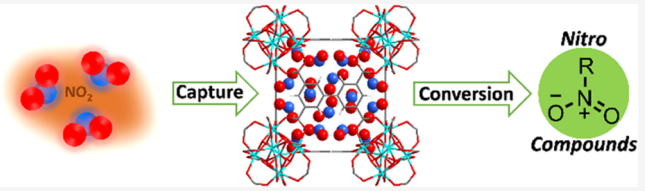

INTRODUCTION

The growing emissions of nitrogen dioxide, NO_2, from the combustion of fossil fuels contribute significantly to global warming, acid rain, and ozone depletion and have severe impacts on the environment and human health.[1−4] State-of-the-art deNO_x processes based upon selective catalytic reduction (SCR) incorporating precious metal catalysts, toxic chemicals, and significant energy consumption[5] are struggling to meet increasingly stringent regulations.[6] The transformation of waste into value-added chemicals is therefore becoming an important target in the development of "circular economy", where products are made, used, and reused, rather than being disposed.[7] Nitro compounds and their derivatives are important intermediates for a wide range of explosives, colorants, agrochemicals, and pharmaceuticals,[8,9] but the state-of-the-art synthesis of nitro compounds relies heavily on the use of HNO_3 and NH_3 that are produced from the extremely energy-demanding Ostwald and Haber−Bosch processes, respectively.[10] The capture and enrichment of pollutant NO_2 and its conversion into nitro compounds are thus a promising route to achieve the circular utilization of reactive nitrogen resources, as well as reducing the carbon footprint for chemical industries.

Exploiting the high porosity and stability of porous materials for the reversible capture of target gases affords economically viable technologies for clean-up and mitigation of gaseous pollutants.[11] Traditional porous materials, such as activated carbons,[12] silica,[13] and zeolites,[14,15] have been tested for the adsorption of NO_2. However, their limited structural stability and restricted design functionalization result in low and often irreversible adsorption. As emerging solid sorbents for a wide spectrum of gases and vapors,[16,17] metal-organic framework (MOF) materials and their composites have been investigated for the adsorption of NO_2.[18] Although some systems have achieved high dynamic sorption (250−2138 ppm) in exceptional cases, the rapid structural degradation of the MOF host upon NO_2 uptake has hampered their further applications (Table S1).[19−24] To the best of our knowledge, only MFM-300(Al)[25] and MFM-520[26] have been reported to display fully reversible NO_2 uptake for the pure gas over repeated cycles. However, MFM-300(Al) shows only a very low uptake of 1.4 mmol g^{-1} at low pressure (10 mbar and 298 K) owing to its inherently moderate binding sites (μ_2-OH and aromatic C−H groups), while MFM-520 exhibits a low total uptake of 4.5 mmol g^{-1} (1.0 bar and 298 K) due to its limited porosity (surface area of 313 m^2 g^{-1}) (Figure S4). To enable the enrichment of NO_2 within pores at low concentrations and the subsequent efficient conversion of NO_2 to nitro compounds, the sorbent material must display high adsorption under both

Received: July 11, 2022
Published: October 5, 2022

https://doi.org/10.1021/jacs.2c07283
J. Am. Chem. Soc. 2022, 144, 18967−18975

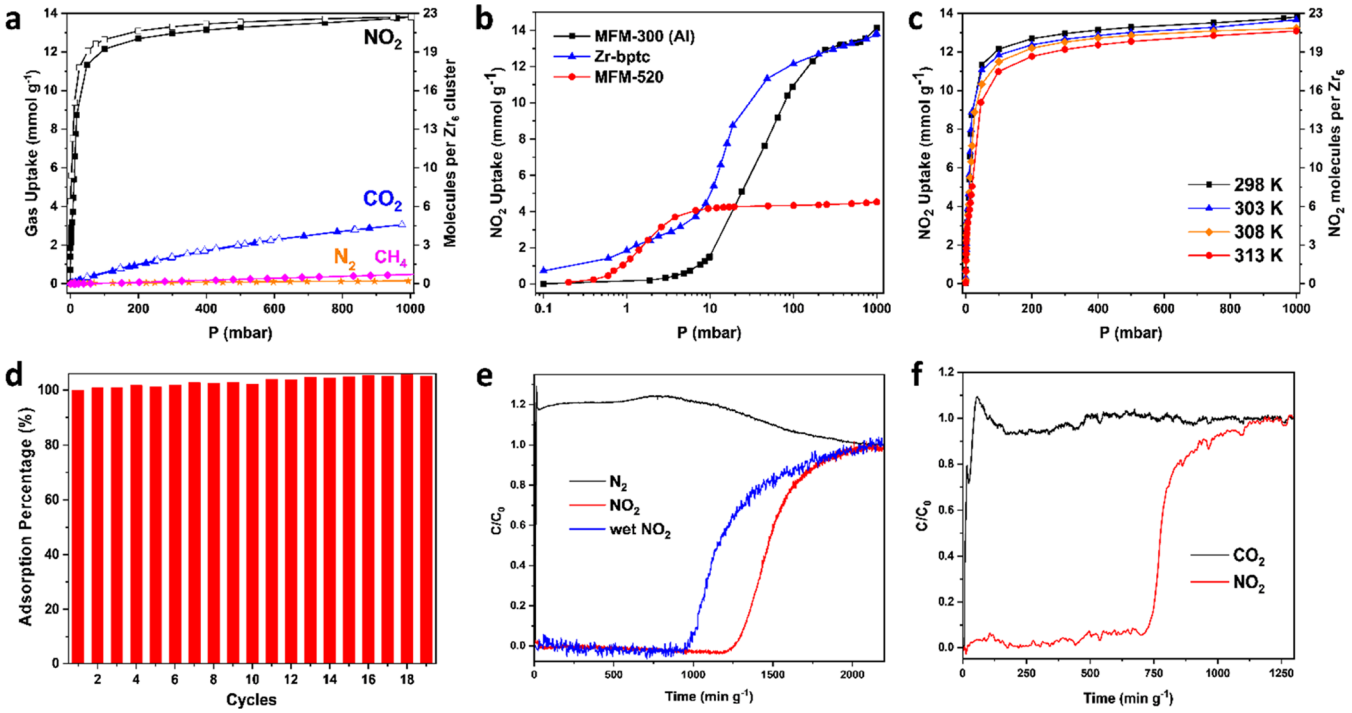

Figure 1. Gas adsorption and dynamic separation data. (a) Adsorption isotherms for NO_2, CO_2, N_2, and CH_4 in desolvated Zr-bptc at 298 K (desorption of N_2 and CH_4 is omitted for clarity); (b) comparison of NO_2 adsorption isotherms on a logarithmic scale for Zr-bptc, MFM-300(Al), and MFM-520 (desorption data are omitted for clarity); (c) sorption isotherms for NO_2 in Zr-bptc (desorption data are omitted for clarity and shown in Figure S5); (d) cyclic adsorption−desorption of NO_2 at 298 K between 0 and 200 mbar (a small gradual increase in the uptake was due to the minor amount of retained NO_2 in Zr-bptc upon desorption under pressure-swing conditions); (e) breakthrough plots for N_2/NO_2 gas mixtures under dry and wet conditions (2500 ppm NO_2 diluted in 77.5% N_2 and 22.25% He); and (f) breakthrough plots for CO_2/NO_2 gas mixtures (2500 ppm NO_2 and 6.25% CO_2 diluted in 93.5% He).

low and high pressures and afford sufficient stability upon regeneration. This represents an extremely challenging target.

Herein, we report the high adsorption of NO_2 in a Zr-based MOF, Zr-bptc, which displays a fully reversible uptake of 4.9 and 13.8 mmol g^{-1} at 10 mbar and 1.0 bar, respectively, at 298 K. In addition, breakthrough experiments confirm that Zr-bptc exhibits highly selective retention of NO_2 at low concentrations (2500 ppm) under both dry and wet conditions. Importantly, the immobilized NO_2 molecules (4.9−13.8 mmol g^{-1}) can be quantitatively converted to various nitro compounds under ambient conditions. The binding domains of NO_2 (and also CO_2 for comparison) in Zr-bptc have been determined by *in situ* synchrotron X-ray powder diffraction. The adsorbed NO_2 molecules partially dimerize to N_2O_4 in the pore, and this has been studied by variable-temperature electron paramagnetic resonance (EPR) spectroscopy. The remaining NO_2 monomers are stabilized by strong host−guest interactions with heats of adsorption (Q_{st}) of 90 kJ mol^{-1}, which have been visualized by *in situ* inelastic neutron scattering (INS) and EPR studies, coupled with density functional theory (DFT) calculations. More importantly, Zr-bptc can be fully regenerated upon the delivery of nitro compounds and reused, thus fulfilling the "waste-to-chemicals" target.

EXPERIMENTAL METHODS

NO_2 Adsorption Isotherms. Gravimetric sorption isotherms of NO_2 were recorded at 298, 303, 308, and 313 K, maintained using a temperature-programmed water bath and furnace, on a Hiden Xemis system under ultrahigh vacuum (10^{-10} bar) using a turbo pumping system. Ultrapure research grade (99.999%) NO_2 was purchased from BOC. In a typical gas adsorption experiment, acetone-exchanged Zr-bptc (50 mg) was loaded into the Xemis system and activated at 573 K under a dynamic high vacuum (10^{-10} bar) for 24 h to give fully desolvated Zr-bptc.

Breakthrough Experiments. The flow rate of the entering gas mixture was maintained at 40 mL min^{-1}, and the gas concentration, C, of gases at the outlet was determined by mass spectrometry and compared with the corresponding inlet concentration C_0, where $C/C_0 = 1$ indicates a complete breakthrough. For breakthrough separation under wet conditions, a fixed bed was packed with Zr-bptc that had been treated and preadsorbed with water at 75% RH. A gas mixture of 0.25% NO_2 (2500 ppm diluted in 22.25% He and 77.5% N_2) was then passed through the fixed bed. Breakthrough separation of NO_2/CO_2 was conducted using a mixture of 0.25% NO_2 (2500 ppm) and 6.25% CO_2 diluted in 93.5% He. The concentrations of NO_2 and CO_2 were chosen to mimic a typical exhaust gas of combustion of diesels in marine transport (N_2: 77.50%, O_2: 13.75%, CO_2: 6.25%, NO_2: 0.212%, SO_2: 0.17%, H_2O: 0.025%, CO: 0.005%, hydrocarbons 0.005%).[27]

General Procedure for Conversion. Preactivated Zr-bptc (1.0 g) was packed in a fixed bed, and a gas flow of 2500 ppm NO_2 (diluted in 77.5% N_2 and 22.25% He) was passed through the column at 298 K until a complete breakthrough was achieved. The gas flow was switched off, and Zr-bptc loaded with 2500 ppm NO_2 (denoted as NO_2@Zr-bptc-N) was sealed for the study of conversion. The quantity of captured NO_2 in NO_2@Zr-bptc-N was determined by TGA, which shows a 19% weight loss between 25 and 330 °C, corresponding to an uptake of 5.1 mmol g^{-1} (Figure S23). This is consistent with that (4.9 mmol g^{-1}) observed in the breakthrough experiment. Aromatic substrates (0.75 mmol) and $CHCl_3$ (5.0 mL) were added to a 10 mL round-bottom flask and stirred for 5 min to obtain a clear solution. NO_2@Zr-bptc-N containing 0.51 mmol NO_2 was added to the solution under stirring at room temperature or 0 °C. Upon completion of the reaction, the mixture was centrifuged, the

https://doi.org/10.1021/jacs.2c07283
J. Am. Chem. Soc. 2022, 144, 18967−18975

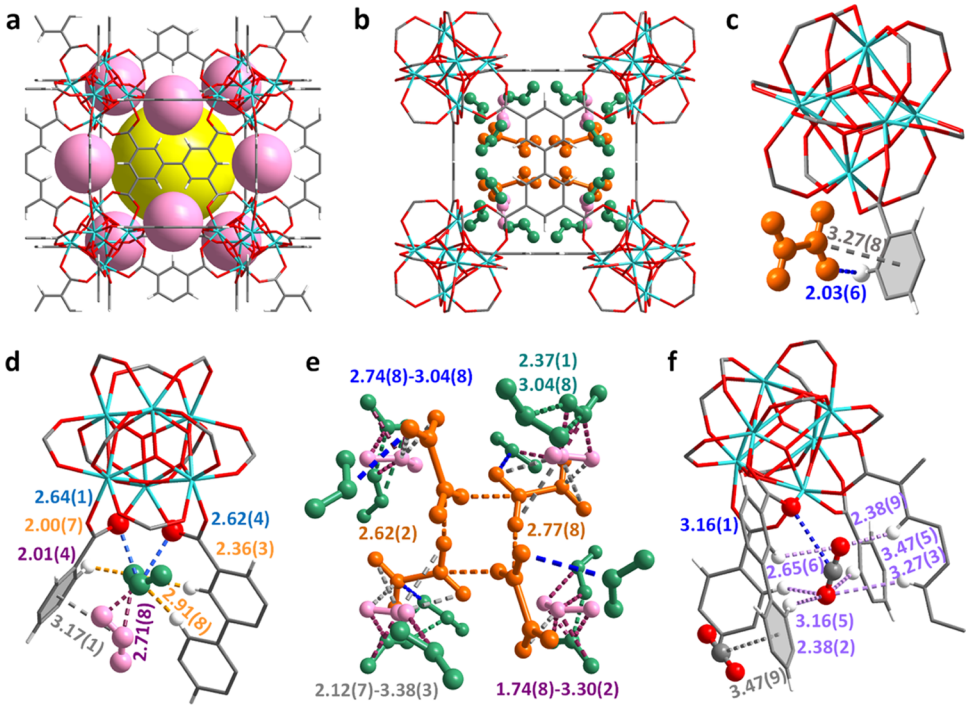

Figure 2. Views of the crystal structures of Zr-bptc, $[Zr_6O_4(OH)_4(bptc)_3{\cdot}(NO_2)_{7.5}{\cdot}(NO_2)_{2.3}{\cdot}(N_2O_4)_{4.1}]$, and $[Zr_6O_4(OH)_4(bptc)_3{\cdot}(CO_2)_{2.8}]$. All structures were derived from Rietveld refinements of *in situ* synchrotron X-ray powder diffraction data collected at 298 K (C: gray; N: blue; O: red Zr: cyan; H: white). (a) Metal−ligand cage A (yellow) and B (rose) in Zr-bptc; (b) packing of adsorbed NO_2 and N_2O_4 molecules in Zr-bptc; (c) enlarged view of binding sites of N_2O_4 in Zr-bptc; (d) enlarged view of the binding site of monomer NO_2 in Zr-bptc; (e) packing of NO_2−N_2O_4 in the pore of Zr-bptc (orange: N_2O_4; sea green: NO_2 at site I; rose: NO_2 at site II; key dipole−dipole interactions are labeled); and (f) enlarged view of the binding site of CO_2 in Zr-bptc.

solid was recycled, and the supernatant was collected and reduced under vacuum for analysis. Nitration experiments were also conducted using Zr-bptc loaded with NO_2 at 1 bar, 298 K (denoted as NO_2@Zr-bptc-N*) (see SI 1.12). The quantity of captured NO_2 in NO_2@Zr-bptc-N* was determined by TGA, which shows a 40% weight loss between 25 and 330 °C, corresponding to an uptake of 14.3 mmol g^{-1} (Figure S23), consistent with that (13.8 mmol g^{-1}) observed in the isotherm adsorption experiments.

RESULTS AND DISCUSSION

The highly stable MOF Zr-bptc $[Zr_6O_4(OH)_4(bptc)_3]$ (H_4bptc = biphenyl-3,3′,5,5′-tetracarboxylic acid) incorporates 12-connected $\{Zr_6(\mu_3\text{-}O)_4(\mu_3\text{-}OH)_4(COO)_{12}\}$ clusters linked by 4-connected $bptc^{4-}$ ligands to form an open and neutral framework in the **ftw** topology.[28] Desolvated Zr-bptc exhibits cubic-shaped cages decorated with $\{Zr_6\}$ clusters and planar $bptc^{4-}$ linkers on the vertices and faces, respectively (denoted as Cage A; Figure 2a). Cage A has a diameter of ∼12 Å after considering the van der Waals' radii, and they are interconnected through another type of smaller tetrahedral cages of ∼4.5 Å diameter (Cage B; Figure 2a) located at the 12 edges of cubic Cage A. The ratio of Cage A to B is 1:3. Desolvated Zr-bptc shows a Brunauer−Emmett−Teller (BET) surface area of 960 m^2 g^{-1}, a pore volume of 0.413 g cm^{-3}, and high chemical, thermal, and water/moisture stability (Figures S1 and S2).

Isothermal adsorption of NO_2 in Zr-bptc reveals exceptional uptakes of 1.8, 4.9, and 13.8 mmol g^{-1} at 0.001, 0.01, and 1.0 bar, respectively, at 298 K (Figures 1a−c and S5). The uptake of NO_2 at very low pressure by Zr-bptc exceeds that of the state-of-the-art material, MFM-520 (1.3 and 4.2 mmol g^{-1} at 0.001 and 0.01 bar, respectively, at 298 K), thus representing a new benchmark for NO_2 adsorption and confirming its potential for the efficient capture of NO_2 at low concentrations. In addition, significant amounts of residual NO_2 (30−50%) were observed upon pressure-swing desorption (Figures 1a and S5), indicating the strong binding of NO_2 in Zr-bptc, which acts as an efficient NO_2 store. Zr-bptc displays a comparable uptake capacity at 1.0 bar with the best-performing material, MFM-300(Al) (14.1 mmol g^{-1} at 298 K),[25] and this high total uptake translates to high working capacities for the storage and conversion of NO_2. Thus, the exceptional uptakes at both very low and ambient pressures endow Zr-bptc with great potential for the development of "waste-to-chemicals" processes. Although a number of metal-doped MOFs[20,24,29] and MOF/graphite oxide composites[23] show the dynamic adsorption of NO_2 (*ca.* 500−1000 ppm) from gas mixtures under both dry and humid conditions, this is not comparable with the direct uptakes obtained *via* isotherm experiments with pure NO_2 owing to the uncertainties in the former, which has been discussed in detail in our earlier report.[25] Furthermore, these composite materials often display partial or complete structural degradation on NO_2 adsorption−desorption cycles. In contrast, little change in structure or sorption capacity was observed for Zr-bptc after 19 cycles of adsorption and desorption of NO_2 (Figures 1d, S1, and S2). Combined thermogravimetric analysis (TGA) and differential scanning calorimetry (DSC) determined the heats of adsorption for NO_2 uptake in Zr-bptc to be 90 kJ mol^{-1} (Figure S9), substantially higher than for MFM-300(Al)[25] and MFM-520(Zn)[26] (61 and 58 kJ mol^{-1}, respectively, determined by TGA−DSC; Figures S10 and S11), thus suggesting the presence of stronger interactions between Zr-bptc and adsorbed NO_2 molecules. This is also consistent with the

https://doi.org/10.1021/jacs.2c07283
J. Am. Chem. Soc. 2022, 144, 18967−18975

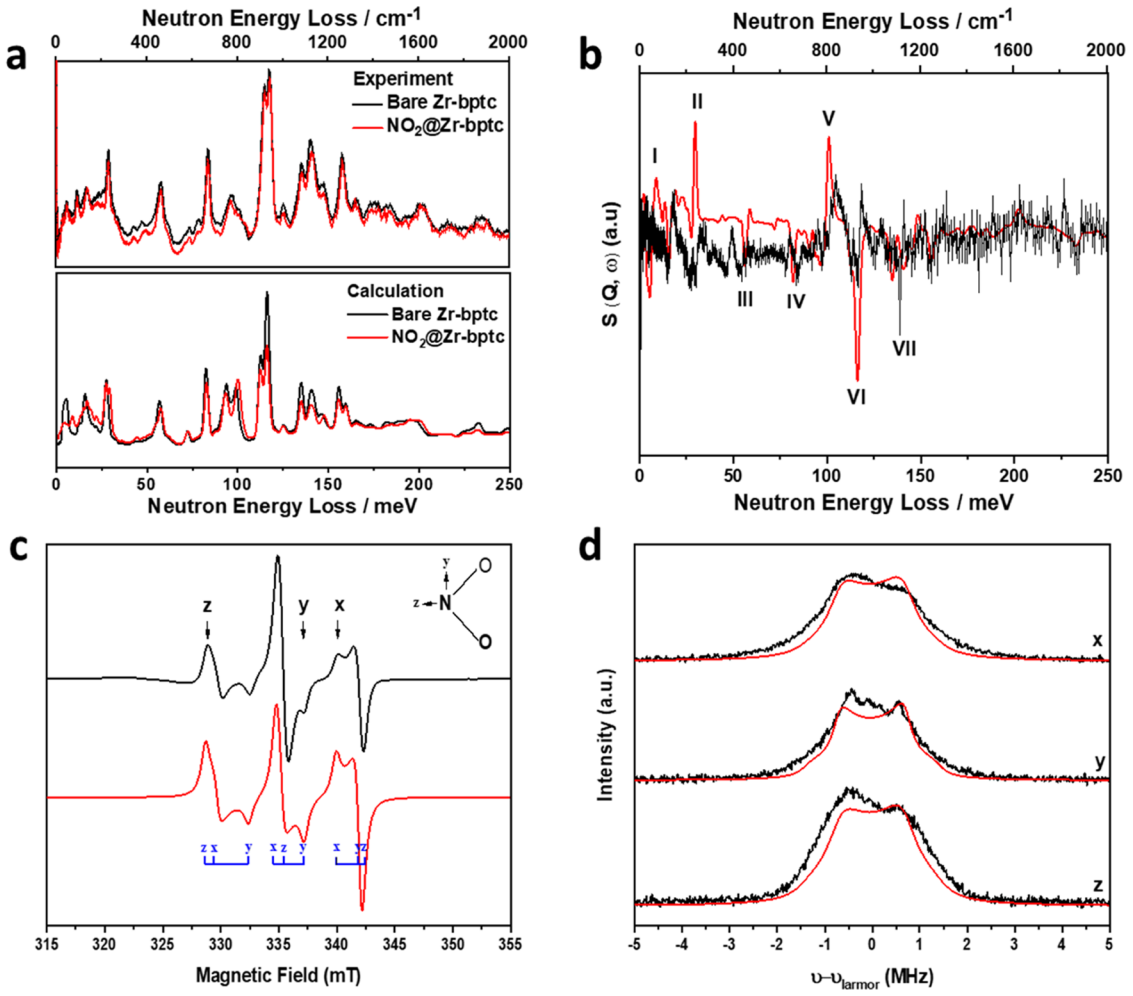

Figure 3. Spectroscopic data. (a) Comparison of the experimental (top) and DFT-simulated (bottom) INS spectra for bare and NO_2-loaded Zr-bptc; (b) comparison of the difference plots for experimental and DFT-calculated INS spectra of bare and NO_2-loaded Zr-bptc. No scale factor was used for the DFT calculations. *S*, dynamic structure factor; *Q*, difference between the incoming and outgoing wave vectors; $\hbar\omega$, the energy change experienced by the sample; (c) continuous-wave X-band (9.72 GHz) EPR spectrum of NO_2@Zr-bptc at 10 K (black) and simulation (red) with g_x = 2.0055, g_y =1.991, and g_z =2.0028 and ^{14}N nuclear hyperfine interactions (nuclear spin, I = 1) of A_x = 145, A_y = 127, and A_z =185 MHz, where *x*, *y*, and *z* define the NO_2 molecular axes (inset). NO_2 has a C_{2v} point symmetry with the z axis along the C_2 rotation axis, *y* parallel to the O−O vector, and x normal to the NO_2 plane; (d) X-band Davies ENDOR spectrum (black) at 5 K and the static magnetic fields indicated, shown by the arrows in panel (c), dominantly selecting the NO_2 *x*, *y*, and *z* axes (top to bottom), respectively. ENDOR gives pairs of transitions separated by the effective hyperfine coupling for the orientation selected, centered on the Larmor frequency of the nucleus being probed (14.9 MHz for ^1H at 350 mT). The black lines are the experimental spectra, and the red lines are the calculated spectra.

higher uptakes observed for Zr-bptc at both low and high pressures. Significantly, Zr-bptc shows low adsorption of CO_2, CH_4, and N_2 at 298 K and 1.0 bar (3.05, 0.49, and 0.14 mmol g^{-1}, respectively) (Figures 1a and S3). The value of Q_{st} for CO_2 uptake is 28 kJ mol^{-1} and shows little variation as a function of surface coverage, indicating weak host−guest interactions (Figures S12 and S13 and Table S2).

Analysis of pure-component isotherms *via* ideal adsorbed solution theory (IAST)[30] affords adsorption selectivities for various gas mixtures (N_2, CO_2, and NO_2) at 298 K and 0−1.0 bar (Figure S14). The IAST selectivities for NO_2/CO_2 (1:99) and NO_2/N_2 (1:99) are ∼750 and >5000, respectively. It is worth noting that the very high IAST selectivities are subject to uncertainties owing to the extremely low adsorption of N_2 or overlapping binding sites of NO_2 and CO_2 in Zr-bptc but confirm the potential of Zr-bptc in the selective adsorption of NO_2 in the presence of CO_2 and N_2. Dynamic breakthrough experiments using a fixed bed packed with Zr-bptc were undertaken with gas mixtures of NO_2/N_2 (2500 ppm NO_2 diluted in 77.5% N_2 and 22.25% He) under both dry and wet (relative humidity: 75%) conditions and with NO_2/CO_2 (2500 ppm NO_2 and 6.25% CO_2 diluted in 93.5% He) at 298 K and 1.0 bar.[27] Highly selective retention of NO_2 by Zr-bptc was observed in all cases, showing a retention time of NO_2 of 1200, 980, and 750 min g^{-1} for the mixture of NO_2/N_2 (dry), NO_2/N_2 (wet), and NO_2/CO_2, respectively (Figure 1e,f) (additional data are shown in Figures S6−S8). Compared with the dynamic adsorption capacity of NO_2 (4.9 mmol g^{-1}) under dry conditions, the small reduction (4.0 mmol g^{-1}) under wet conditions is due to the competitive adsorption of water and reaction between adsorbed NO_2 and H_2O molecules in the pore. The dynamic selectivities of NO_2/N_2 and NO_2/CO_2 are estimated to be 151 and 24, respectively.

Rietveld refinement of the high-resolution synchrotron X-ray powder diffraction data of NO_2-loaded Zr-bptc, $[Zr_6O_4(OH)_4(bptc)_3{\cdot}(NO_2)_{7.5}{\cdot}(NO_2)_{2.3}{\cdot}(N_2O_4)_{4.1}]$, at 298 K

https://doi.org/10.1021/jacs.2c07283
J. Am. Chem. Soc. 2022, 144, 18967−18975

revealed three independent binding sites, I, II, and III, which are assigned as NO_2, NO_2, and N_2O_4 molecules, respectively (Figures 2b, S15, and S20 and Table S3). The total crystallographic occupancy of NO_2 molecules (18.0 NO_2 per $\{Zr_6\}$ cluster) is slightly lower than that obtained from the isotherm (22.9 NO_2 per $\{Zr_6\}$ cluster), which is likely due to the presence of a small amount of highly disordered NO_2 molecules in the pores. The NO_2 molecules at site I (7.5 NO_2 per $\{Zr_6\}$ cluster) exhibit strong interaction with the carboxylate group [$O_2\underline{N}\cdots\underline{O}OC$ = 2.64(1) and 2.62(4) Å] (Figure 2d). Furthermore, O centers from NO_2 molecules form multiple supramolecular interactions with the aromatic C−H groups on benzene rings. The interaction [$N\underline{O}_2\cdots\underline{H}-C$ = 2.00(7)], <C−H−O = 101.8(4)° and twofold hydrogen bond [$N\underline{O}_2\cdots\underline{H}-C$ = 2.36(3), 2.91(8) Å, <C−H−O = 144.4(7), 156.5(7)°] (Table S4) stabilize the packing of NO_2 molecules at site I. The multiple hydrogen bonds and dipole−dipole interactions between NO_2 at site I and the framework suggest strong binding, consistent with the exceptionally high adsorption at low pressure. Three different dipole interactions including [$O_2\underline{N}\cdots$benzene = 3.17(1) Å] and [$N\underline{O}_2\cdots\underline{N}O_2$ = 2.01(4) and 2.71(8) Å] stabilize the NO_2 molecules at site II (2.3 NO_2 per $\{Zr_6\}$ cluster). Interestingly, NO_2 molecules at site III (8.2 NO_2 per $\{Zr_6\}$ cluster) are dimerized to N_2O_4 and stabilized by electrostatic and dipole interactions [$N_2\underline{O}_4\cdots\underline{H}-C$ = 2.03(6) and $O_2\underline{N}\cdots$benzene = 3.27(8) Å] (Figure 2c). The packing of NO_2−N_2O_4 molecules is sustained by multiple intermolecular dipole−dipole interactions based upon monomer-to-monomer, monomer-to-dimer, and dimer-to-dimer with distances ranging from 1.74(8) to 3.38(3) Å, offering an efficient storage environment (Figure 2e), consistent with the high Q_{st} of Zr-bptc (90 kJ mol^{-1}). Interestingly, the NO_2 and N_2O_4 molecules immobilized in the pores of Zr-bptc on saturation show an unprecedented packing density of 1.83 g cm^{-3} at 298 K, higher than that observed in MFM-300(Al) (1.73 g cm^{-3} at 298 K), MFM-520 (1.42 g cm^{-3} at 298 K), liquid NO_2 and N_2O_4 (1.45 and 1.44 g cm^{-3}, respectively, at 294 K), and close to that of solid N_2O_4 (1.94 g cm^{-3} at 140 K).[31] This result confirms a highly efficient packing of NO_2/N_2O_4 molecules within the pores of Zr-bptc.

Two independent binding sites, I' and II', were located in cages B and A, respectively, in CO_2-loaded Zr-bptc, $[Zr_6O_4(OH)_4(bptc)_3\cdot(CO_2)_{2.8}]$ (Figures S16−S19). The total crystallographic occupancy of 2.8 CO_2 per $\{Zr_6\}$ cluster is lower than that obtained from the isotherm (5.2 CO_2 per $\{Zr_6\}$ cluster), likely due to the presence of a large amount of highly disordered CO_2 molecules in the pore owing to the weak host−guest interactions. CO_2 molecules at site I' (0.93 CO_2 per $\{Zr_6\}$ cluster) display dipole interactions with the carboxylate group [$O_2\underline{C}\cdots\underline{O}OC$ = 3.16(1) Å] (Figure 2f). In addition, multiple weak supramolecular interactions were observed between $CO_2^{I'}$ molecules and the benzene ring [$O{=}C{=}\underline{O}\cdots\underline{H}-C$ = 2.38(2)−3.47(5) Å] (Table S4). The CO_2 molecules at site II' (1.87 CO_2 per $\{Zr_6\}$ cluster) are stabilized by the $\pi\cdots\pi$ interaction with the phenyl ring [$O_2\underline{C}\cdots$benzene = 3.47(9) Å]. Overall, the host−guest binding interaction is notably weaker than that of NO_2, consistent with low Q_{st} (28 kJ mol^{-1}) and the selective uptake of NO_2 in the breakthrough experiment.

In situ INS, coupled with DFT calculations, enabled the visualization of the binding dynamics for NO_2-loaded Zr-bptc with a focus on the −CH groups involved in the supramolecular contacts. Seven major changes in the INS spectra were observed on the adsorption of NO_2 in Zr-bptc (Figure 3a,b). Peaks I−III at low energy transfer (<60 meV) and peaks IV−VII at high energy (80−150 meV) correspond to deformational modes of the phenyl ring and the twisting/wagging/scissoring modes of the aromatic −CH groups, respectively. These changes support the direct interactions between adsorbed NO_2/N_2O_4 molecules and the soft −CH groups, consistent with the *in situ* crystallographic analysis.

The presence of adsorbed NO_2 monomers in Zr-bptc is confirmed unambiguously by EPR spectroscopy on NO_2@Zr-bptc at 10 K (Figure 3c), which shows signals for immobilized NO_2 with a resolution of both the anisotropic electronic *g*-factor and ^{14}N hyperfine interaction.[32] The spectral line width is approximately double that of NO_2-loaded MFM-300(Al)[25] (Table S5), reflecting the higher concentration of monomeric NO_2 in the pores of Zr-bptc, as found by the crystallographic study. The interaction of NO_2 with the framework was probed by Davies ENDOR (electron−nuclear double resonance) spectroscopy at 5.7 K, which reveals weak ^1H hyperfine interactions with frequencies around 2 MHz (Figure 3d).[33] Based on a point-dipole model, these can be reproduced with a $H\cdots\underline{N}O_2$ distance of 3.8 Å. The ENDOR spectra are rather broad and relatively insensitive to the magnetic field of measurement, *i.e.*, with respect to the orientation of the NO_2 molecule. This is presumably because of the multiple monomer NO_2 binding sites within the pores of Zr-bptc; much stronger orientation selection is observed for NO_2@MFM-300(Al) system, which has only one monomer binding site. This result is consistent with the enhanced packing density of NO_2 in Zr-bptc. The $H\cdots\underline{N}O_2$ distance from ENDOR at 10 K is longer than that found from the structural model determined at room temperature, indicating that the trapped NO_2 molecules form stronger intermolecular interactions at low temperature. On warming the sample (200−360 K; Figure S21), the spectra broaden and the signal intensity increases as a function of the monomer−dimer equilibrium in the pores.[26]

Nitration is widely used in the chemical industry to produce important nitro compounds (*e.g.*, nitrobenzene), which are key intermediates for the synthesis of a wide range of explosives, colorants, agrochemicals, and pharmaceuticals.[8,9,26,34] The global market for nitrobenzene is $9.8 billion in 2020 and is projected to reach $14.5 billion by 2027.[35] The construction industry is the dominant end user of nitrobenzene and consumes approximately half of the world's annual production. In addition, nitrobenzene is also used in the synthesis of paracetamol, which serves as a generic medicine globally. For other examples, nifedipine, entacapone, and niclosamide are nitro-group-containing medicines and are widely used to treat hypertension, Parkinson's disease, and tapeworm infections, respectively.[36] Nitration in the chemical industry is usually carried out using a mixture of concentrated acids (*e.g.*, 20% nitric acid, 60% sulfuric acid, and 20% water for mononitration) at 80−120 °C.[9] Because these processes are highly exothermic, enormous amounts of energy are consumed by cooling. Additionally, the industrial production of nitric acid *via* the oxidation of ammonia in the Ostwald process carries huge carbon footprints.[10] Thus, nitration is widely considered one of the most energy-consuming and hazardous industrial processes. Although NO_2 gas can be used as a nitration reagent, its highly corrosive and toxic nature renders the operation highly challenging.[39] In addition, byproducts from overnitration and overoxidation are often obtained when using

https://doi.org/10.1021/jacs.2c07283
J. Am. Chem. Soc. 2022, 144, 18967−18975

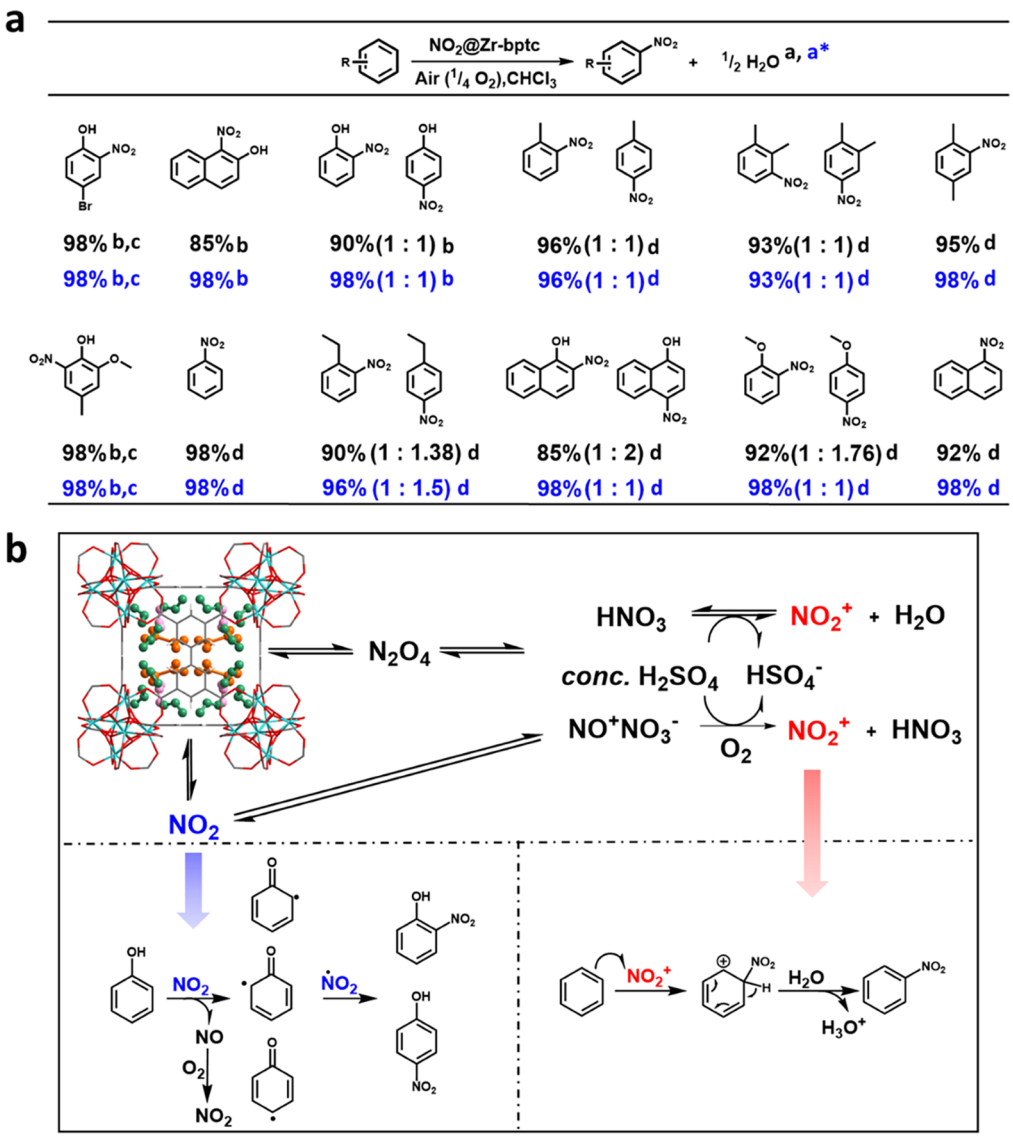

Figure 4. Schematic view of the utilization of NO_2 pollutant for nitration processes. (a) Views of nitro compounds prepared using captured NO_2. Yields are based on the captured NO_2. [a]NO_2@Zr-bptc-N was formed from Zr-bptc loaded with NO_2 at 2500 ppm at 298 K to give a total capacity of NO_2 of 5.1 mmol g^{-1}. Conditions for nitration: a sample of NO_2@Zr-bptc-N containing 0.51 mmol of NO_2 was treated with 0.75 mmol of aromatic substrate in 5 mL of $CHCl_3$ at room temperature. Yields and selectivity are in black. [a*]NO_2@Zr-bptc-N* was formed from Zr-bptc loaded with NO_2 at 1 bar at 298 to give a total capacity of NO_2 of 14.3 mmol g^{-1}. A sample of NO_2@Zr-bptc-N* containing 1.43 mmol of NO_2 was treated with 1.5 mmol of aromatic substrate in 5 mL of CH_2Cl_2 at room temperature. Yields and selectivity are in blue. [b]Reaction conducted at 0 °C within 0.5 h; [c]the reaction was completed within 1.0 h; [d]a catalytic amount (1%) of *conc.* H_2SO_4 was added, and the reaction time was extended to 6.0 h; (b) proposed mechanism for the nitration reaction of phenol and benzene by NO_2@Zr-bptc-N. The captured NO_2 is released from the MOF into the reaction mixture as N_2O_4 or NO_2. In the presence of *conc.* H_2SO_4, NO_2^+ is produced in the presence of O_2, which drives the nitration process. For the nitration process in the absence of *conc.* H_2SO_4, the reaction occurs between NO_2-derived radicals and substrate.[37,38] The MOF plays a key role in the enrichment of NO_2 from gas mixtures and facile release of captured NO_2 into the reaction system.

gaseous or liquid NO_2 in nitration processes,[40,41] and this is also confirmed by our tests on the nitration of a range of substrates with NO_2 gas (Figures S27−S36). We sought to convert the captured NO_2 by Zr-bptc to valuable nitro compounds at room temperature and without the use of mixtures of concentrated acids. Activated Zr-bptc was loaded with NO_2 at 2500 ppm, which gives an uptake of 5.1 mmol g^{-1} (denoted as NO_2@Zr-bptc-N; see the Experimental Methods and SI sections for details). Activated Zr-bptc was also loaded with NO_2 at 1 bar, which gives an uptake of 14.3 mmol g^{-1} (denoted as NO_2@Zr-bptc-N*; see the Experimental Methods and SI sections for details). A series of nitration experiments of aromatic compounds were then undertaken using NO_2@Zr-bptc-N as the nitration source (Figures 4a and S37−S69). A fixed amount of NO_2@Zr-bptc-N (containing 0.51 mmol NO_2) was added to the mixture of aromatic substrates (0.75 mmol) and $CHCl_3$ (5.0 mL) under stirring at room temperature or 0 °C, and the product was isolated by centrifugation and the supernatant was collected and analyzed by NMR spectroscopy. Importantly, the captured NO_2 molecules can be quantitatively converted to nitro compounds in the absence or the presence of a catalytic amount (1%) of sulfuric acid, which is also confirmed by EPR analysis of the postreaction mixture that confirms the absence of residual NO_2 (Fig. S24). Mononitration was achieved in a series of key aromatic compounds, including benzene, naphthalene, and

https://doi.org/10.1021/jacs.2c07283
J. Am. Chem. Soc. 2022, 144, 18967−18975

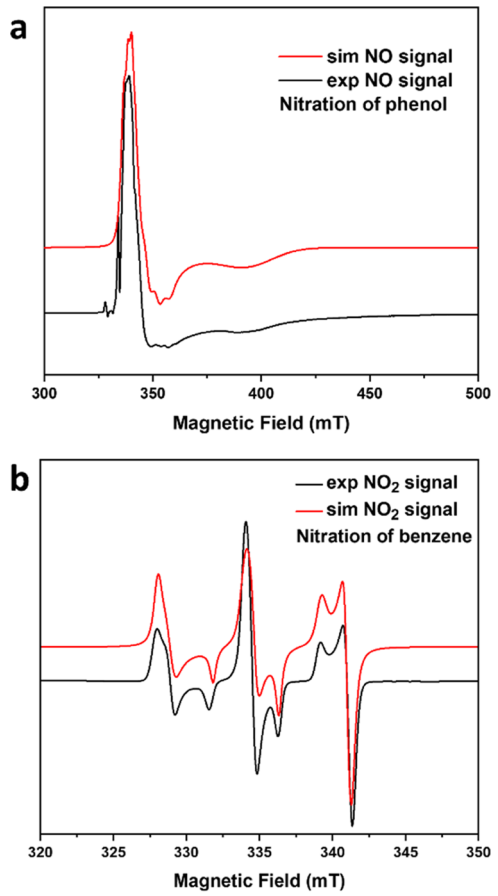

Figure 5. EPR spectroscopy. (a) Continuous-wave X-band (9.72 GHz) EPR spectra of the nitration reaction mixture of phenol at 10 K (black) and simulation (red); and (b) continuous-wave X-band (9.72 GHz) EPR spectra of the nitration reaction mixture of benzene at 10 K (black) and simulation (red), confirming the absence of NO.

p-xylene with yields of >85%. *O*- and *p*-substituted nitro compounds were obtained in nearly 1:1 ratio for phenol, toluene, and *o*-xylene and >1:1.4 ratio for ethylbenzene, anisole, and naphthalen-2-ol. Trace amounts of *m*-substituted nitro compound, which is a common product in the nitration process with gaseous NO_2,[40,41] were observed in these reactions. Control experiments using H_4bptc or $ZrOCl_2 \cdot 8H_2O$ as the capture material were conducted, and little conversion was observed (Figure S26), demonstrating the key role of Zr-bptc in enriching NO_2 from gas mixtures and releasing NO_2 into the reaction medium (Figure S25).

In addition, EPR spectroscopy was employed to validate the proposed mechanism (Figure 4b), and the presence of signals of NO in the nitration of phenol demonstrated the presence of an alternative reaction pathway to nitronium ion-induced nitration, consistent with the short reaction time required (Figure 5a,b). The Zr-bptc recovered from these reactions can be regenerated fully *via* heating under dynamic vacuum. Uptake of NO_2 and conversion efficiency in the synthesis of nitrobenzene were stable over three consecutive cycles (Figures S2 and S70 and Table S6). Thus, the integration of waste NO_2 into the production of important nitro compounds not only holds the promise to reduce the carbon footprint of existing industrial nitration processes but also fulfills the requirement of "waste-to-chemicals" processes (Figure 6).

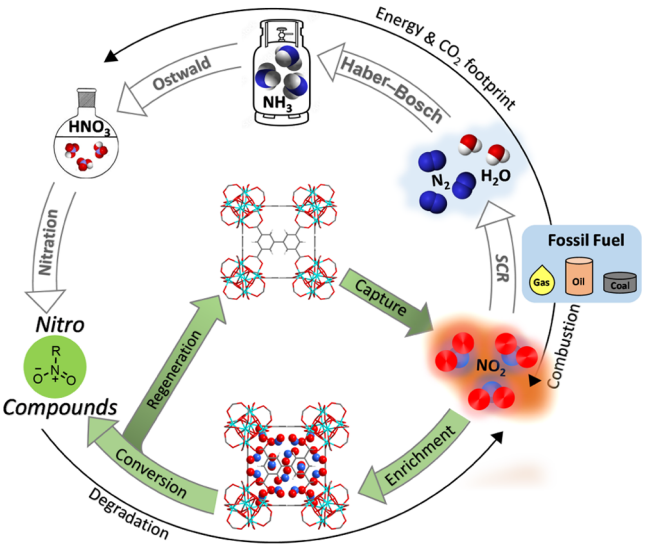

Figure 6. Illustration of the nitrogen cycle for the synthesis of nitro compounds and regeneration of sorbent materials.

CONCLUSIONS

The robust porous MOF material, Zr-bptc, exhibits exceptional adsorption capacity of NO_2 under both low- and high-pressure conditions and high heats of adsorption with an unprecedented packing density of NO_2 in the pore. *In situ* synchrotron X-ray diffraction and INS studies, coupled with DFT calculations, unravel the molecular details on the host–guest binding that result in excellent adsorption performance. *In situ* EPR analysis demonstrates the existence of NO_2–N_2O_4 equilibrium in this system. The successful synthesis of various fine chemicals from the key air pollutant demonstrates a promising "waste-to-chemicals" process for the recovery and circular utilization of reactive nitrogen-based wastes.

ASSOCIATED CONTENT

Supporting Information

The Supporting Information is available free of charge at https://pubs.acs.org/doi/10.1021/jacs.2c07283.

Additional crystallographic information, gas adsorption data, thermogravimetric analysis, density functional theory (DFT) calculations, breakthrough data, stability test data, and conversion of captured NO_2 are available (PDF)

Accession Codes

CCDC 2118350, 2118669, and 2120007 contain the supplementary crystallographic data for this paper. These data can be obtained free of charge via www.ccdc.cam.ac.uk/data_request/cif, or by emailing data_request@ccdc.cam.ac.uk, or by contacting The Cambridge Crystallographic Data Centre, 12 Union Road, Cambridge CB2 1EZ, UK; fax: +44 1223 336033.

AUTHOR INFORMATION

Corresponding Authors

Martin Schröder – *Department of Chemistry, University of Manchester, Manchester M13 9PL, U.K.*; orcid.org/0000-0001-6992-0700; Email: M.Schroder@manchester.ac.uk

Sihai Yang – *Department of Chemistry, University of Manchester, Manchester M13 9PL, U.K.*; orcid.org/0000-0002-1111-9272; Email: Sihai.Yang@manchester.ac.uk

Authors

Jiangnan Li − *Department of Chemistry, University of Manchester, Manchester M13 9PL, U.K.*

Zi Wang − *Department of Chemistry, University of Manchester, Manchester M13 9PL, U.K.*

Yinlin Chen − *Department of Chemistry, University of Manchester, Manchester M13 9PL, U.K.*

Yongqiang Cheng − *Neutron Scattering Division, Neutron Sciences Directorate, Oak Ridge National Laboratory, Oak Ridge, Tennessee 37831, United States;* orcid.org/0000-0002-3263-4812

Luke L. Daemen − *Neutron Scattering Division, Neutron Sciences Directorate, Oak Ridge National Laboratory, Oak Ridge, Tennessee 37831, United States*

Floriana Tuna − *Department of Chemistry, University of Manchester, Manchester M13 9PL, U.K.; Photon Science Institute, University of Manchester, Manchester M13 9PL, U.K.*

Eric J. L. McInnes − *Department of Chemistry, University of Manchester, Manchester M13 9PL, U.K.;* orcid.org/0000-0002-4090-7040

Sarah J. Day − *Diamond Light Source, Harwell Science Campus, Oxfordshire OX11 0DE, U.K.*

Anibal J. Ramirez-Cuesta − *Neutron Scattering Division, Neutron Sciences Directorate, Oak Ridge National Laboratory, Oak Ridge, Tennessee 37831, United States*

Complete contact information is available at: https://pubs.acs.org/10.1021/jacs.2c07283

Notes

The authors declare no competing financial interest.

■ ACKNOWLEDGMENTS

The authors thank EPSRC (EP/I011870), the Royal Society, and the University of Manchester for funding. This project has received funding from the European Research Council (ERC) under the European Union's Horizon 2020 research and innovation program (grant agreement No. 742401, NANOCHEM). The authors are grateful to Diamond Light Source and Oak Ridge National Laboratory (ORNL) for access to Beamlines I11 and VISION (a DOE Office of Science User Facility), respectively. The computing resources were made available through the VirtuES and the ICE-MAN projects, funded by Laboratory Directed Research and Development program and Compute and Data Environment for Science (CADES) at ORNL. We acknowledge EPSRC for funding the UK National EPR Facility.

■ REFERENCES

(1) Lee, M.; Shevliakova, E.; Stock, C.; Malyshev, A. S.; Milly, C. D. P. Prominence of the tropics in the recent rise of global nitrogen pollution. *Nat. Commun.* **2019**, *10*, No. 1437.

(2) Editorial. Clean air for a sustainable world. *Nat. Commun.* 2021, *12*, 5824.

(3) Wall, D. H.; Nielsen, U. N.; Six, J. Soil biodiversity and human health. *Nature* **2015**, *528*, 69−76.

(4) Aravkin, A. Y.; GBD Global Risk Factors Collaborators; et al. Global burden of 87 risk factors in 204 countries and territories, 1990−2019: a systematic analysis for the global burden of disease study 2019. *Lancet* **2020**, *396*, 1223−1249.

(5) Mladenović, M.; Paprika, M.; Marinković, A. Denitrification techniques for biomass combustion. *Renewable Sustainable Energy Rev.* **2018**, *82*, 3350−3364.

(6) WHO global air quality guidelines: particulate matter (PM2.5 and PM10), ozone, nitrogen dioxide, sulfur dioxide and carbon monoxide. https://apps.who.int/iris/handle/10665/345329?locale-attribute=pt& World Health Organization (2021) (accessed July, 2022).

(7) Iaquaniello, G.; Centi, G.; Salladini, A.; Palo, E.; Perathoner, S. Waste to chemicals for a circular economy. *Chem. - Eur. J.* **2018**, *24*, 11831−11839.

(8) Nepali, K.; Lee, H. Y.; Liou, J. P. Nitro-group-containing drugs. *J. Med. Chem.* **2019**, *62*, 2851−2893.

(9) Booth, G. Nitro Compounds, Aromatic. In *Ullmann's Encyclopaedia of Industrial Chemistry*; Wiley, 1988.

(10) Chen, J. G.; Crooks, M. R.; Seefeldt, C. L.; Bren, L. K.; Bullock, M. R.; Darensbourg, Y. M.; Holland, L. P.; Hoffman, B.; Janik, J. M.; Jone, K. A.; Kanatzidis, G. M.; King, P.; Lancaste, M. K.; Lymar, V. S.; Pfromm, P.; Schneider, F. W.; Schrok, R. R. Beyond fossil fuel-driven nitrogen transformations. *Science* **2018**, *360*, No. eaar6611.

(11) Wang, H.; Wang, M.; Liang, X.; Yuan, J.; Yang, H.; Wang, S.; Ren, Y.; Wu, H.; Pan, F.; Jiang, Z. Organic molecular sieve membranes for chemical separations. *Chem. Soc. Rev.* **2021**, *50*, 5468−5516.

(12) Abdulrasheed, A. A.; Jalil, A. A.; Triwahyono, S.; Zaini, A. A. M.; Gambo, Y.; Ibrahim, M. Surface modification of activated carbon for adsorption of SO_2 and NO_x: A review of existing and emerging technologies. *Renewable Sustainable Energy Rev.* **2018**, *94*, 1067−1085.

(13) Ko, G. J.; Ham, D. S.; Kim, K. J.; Zhu, J.; Han, B. W.; Chung, J.; Yang, M. S.; Cheng, H.; Kim, H. D.; Kang, Y. C.; Hwang, W. S. Biodegradable, flexible silicon nanomembrane-based NO_x gas sensor system with record-high performance for transient environmental monitors and medical implants. *NPG Asia Mater.* **2020**, *12*, No. 71.

(14) Wang, X.; Hanson, J. C.; Kwak, J. H.; Szanyi, J.; Peden, C. H. Cation movements during dehydration and NO_2 desorption in a Ba−Y, FAU zeolite: an *in situ* time-resolved X-ray diffraction study. *J. Phys. Chem. C* **2013**, *117*, 3915−3922.

(15) Franus, M.; Wdowin, M.; Bandura, L.; Franus, W. Removal of environmental pollutions using zeolites from fly ash: A review. *Fresenius Environ. Bull.* **2015**, *24*, 854−866.

(16) Woellner, M.; Hausdorf, S.; Klein, N.; Mueller, P.; Smith, W. M.; Kaskel, S. Adsorption and detection of hazardous trace gases by metal−organic frameworks. *Adv. Mater.* **2018**, *30*, No. 1704679.

(17) Liang, Z.; Qu, C.; Guo, W.; Zou, R.; Xu, Q. Pristine metal−organic frameworks and their composites for energy storage and conversion. *Adv. Mater.* **2018**, *30*, No. 1702891.

(18) Han, X.; Yang, S.; Schröder, M. Porous metal−organic frameworks as emerging sorbents for clean air. *Nat. Rev. Chem.* **2019**, *3*, 108−118.

(19) Peterson, G. W.; Mahle, J. J.; Decoste, J. B.; Gordon, W. O.; Rossin, J. A. Extraordinary NO_2 removal by the metal-organic framework UiO-66-NH_2. *Angew. Chem., Int. Ed.* **2016**, *55*, 6235−6238.

(20) Shang, S.; Yang, C.; Wang, C.; Qin, J.; Li, Y.; Gu, Q.; Shang, J. Transition metal inserted porphyrin metal-organic frameworks as π-backbonding adsorbents for NO_2 removal. *Angew. Chem., Int. Ed.* **2020**, *59*, 19680−19683.

(21) Wang, Y.; Liu, D.; Yin, J.; Shang, Y.; Du, J.; Kang, Z.; Wang, R.; Chen, Y.; Sun, D.; Jiang, J. An ultrafast responsive NO_2 gas sensor based on a hydrogen-bonded organic framework material. *Chem. Commun.* **2020**, *56*, 703−706.

(22) Ebrahim, A. M.; Levasseur, B.; Bandosz, T. J. Interactions of NO_2 with Zr-Based MOF: Effects of the size of organic linkers on NO_2 adsorption at ambient conditions. *Langmuir* **2013**, *29*, 168−174.

(23) Levasseur, B.; Petit, C.; Bandosz, T. J. Reactive adsorption of NO_2 on copper-based metal-organic framework and graphite oxide/metal-organic framework composites. *ACS Appl. Mater. Interfaces* **2010**, *2*, 3606−3613.

(24) Ebrahim, A. M.; Bandosz, T. J. Ce(III) doped Zr-based MOFs as excellent NO_2 adsorbents at ambient conditions. *ACS Appl. Mater. Interfaces* **2013**, *5*, 10565−10573.

(25) Han, X.; Godfrey, G. W. H.; Briggs, L.; Davies, J. A.; Cheng, Y.; Daemen, L. L.; Sheveleva, M. A.; Tuna, F.; McInnes, J. L. E.; Sun, J.; Drathen, C.; George, W. M.; Ramirez-Cuesta, J. A.; Thomas, M. K.; Yang, S.; Schröder, M. Reversible adsorption of nitrogen dioxide within a robust porous metal−organic framework. *Nat. Mater.* **2018**, *17*, 691−696.
(26) Li, J.; Han, X.; Zhang, X.; Sheveleva, M. A.; Cheng, Y.; Tuna, F.; McInnes, J. L. E.; McPherson, J. M. L.; Teat, J. S.; Daemen, L. L.; Ramirez-Cuesta, J. A.; Schröder, M.; Yang, S. Capture of nitrogen dioxide and conversion to nitric acid in a porous metal−organic framework. *Nat. Chem.* **2019**, *11*, 1085−1090.
(27) Seddiek, I. S.; Elgohary, M. M. Eco-friendly selection of ship emissions reduction strategies with emphasis on SO_x and NO_x emissions. *Int. J. Nav. Archit. Ocean Eng.* **2014**, *6*, 737−748.
(28) Wang, H.; Dong, X.; Lin, J.; Teat, J. S.; Jensen, S.; Cure, J.; Alexandrov, V. E.; Xia, Q.; Tan, K.; Wang, Q.; Olson, H. D.; Proserpio, M. D.; Chabal, J. Y.; Thonhauser, T.; Sun, J.; Han, Y.; Li, J. Topologically guided tuning of Zr-MOF pore structures for highly selective separation of C6 alkane isomers. *Nat. Commun.* **2018**, *9*, No. 1745.
(29) Ebrahim, A. M.; Bandosz, T. J. Effect of amine modification on the properties of zirconium-carboxylic acid based materials and their applications as NO_2 adsorbents at ambient conditions. *Microporous Mesoporous Mater.* **2014**, *188*, 149−162.
(30) Myers, A. L.; Prausnitz, J. M. Thermodynamics of mixed-gas adsorption. *AlChE J.* **1965**, *11*, 121−127.
(31) Kvick, Å.; McMullan, R. K.; Newton, M. D. The structure of dinitrogen tetroxide N_2O_4: neutron diffraction study at 100, 60, and 20 K and *ab initio* theoretical calculations. *J. Chem. Phys.* **1982**, *76*, 3754−3761.
(32) Shiotani, M.; Moro, G.; Freed, J. H. ESR studies of NO_2-adsorbed on Ti supported surfaces: Analysis of motional dynamics. *J. Chem. Phys.* **1981**, *74*, 2616−2640.
(33) Kulik, L.; Lubitz, W. Electron-nuclear double resonance. *Photosynth. Res.* **2009**, *102*, 391−401.
(34) Patai, S. *The Chemistry Of Amino, Nitroso And Nitro Compounds And Their Derivatives*; The Hebrew University: Jerusalem, 1982.
(35) Nitrobenzene Market Size, Share & Trends Analysis Report By Application (Aniline Production, Synthetic Rubber Manufacturing), By End Use (Construction, Automotive), By Region, And Segment Forecasts, 2020 − 2027. https://www.grandviewresearch.com/industry-analysis/nitrobenzene-market (accessed July, 2022).
(36) Nepali, K.; Lee, Y. H.; Liou, P. J. Nitro-group-containing drugs. *J. Med. Chem.* **2019**, *62*, 2851−2893.
(37) Misiaszek, R.; Crean, C.; Geacintov, E. N.; Shafirovich, V. Combination of nitrogen dioxide radicals with 8-oxo-7, 8-dihydroguanine and guanine radical in DNA: oxidation and nitration end-products. *J. Am. Chem. Soc.* **2005**, *127*, 2191−2200.
(38) Deng, R.; You, K.; Ni, W.; Zhao, F.; Liu, P.; Luo, H. Low-temperature and highly efficient liquid-phase catalytic nitration of chlorobenzene with NO_2: remarkably improving the para-selectivity in O_2-Ac_2O-Hβ composite system. *Appl. Catal., A* **2020**, *594*, No. 117468.
(39) Bosch, E.; Kochi, J. K. Thermal and photochemical nitration of aromatic hydrocarbons with nitrogen dioxide. *J. Org. Chem.* **1994**, *59*, 3314−3325.
(40) Mori, T.; Suzuki, H. Ozone-mediated nitration of aromatic compounds with lower oxides of nitrogen (the Kyodai nitration). *Synlett* **1995**, *1995*, 383−392.
(41) Qi, X.; Cheng, G.; Lu, C.; Qian, D. Nitration of simple aromatics with NO_2 under air atmosphere in the presence of novel brønsted acidic ionic liquids. *Synth. Commun.* **2008**, *38*, 537−545.

https://doi.org/10.1021/jacs.2c07283
J. Am. Chem. Soc. 2022, 144, 18967−18975